Time reversal focusing of elastic waves in plates for an educational demonstration

Christopher Heaton, Brian E. Anderson, and Sarah M. Young

Time reversal focusing of elastic waves in plates for an educational demonstration

Christopher Heaton, Brian E. Anderson,[a)] and Sarah M. Young

Acoustics Research Group, Department of Physics and Astronomy, Brigham Young University, Provo, Utah 84602, USA

The purpose of this research is to develop a visual demonstration of time reversal focusing of vibrations in a thin plate. Various plate materials are tested to provide optimal conditions for time reversal focusing. Specifically, the reverberation time in each plate and the vibration coupling efficiency from a shaker to the plate are quantified to illustrate why a given plate provides the best spatially confined focus as well as the highest focal amplitude possible. A single vibration speaker and a scanning laser Doppler vibrometer (SLDV) are used to provide the time reversal focusing. Table salt is sprinkled onto the plate surface to allow visualization of the high amplitude, spatially localized time reversal focus; the salt is thrown upward only at the focal position. Spatial mapping of the vibration focusing on the plate using the SLDV is correlated to the visual salt jumping demonstration. The time reversal focusing is also used to knock over an object when the object is placed at the focal position; some discussion of optimal objects to use for this demonstration are given.
© 2017 Acoustical Society of America. [http://dx.doi.org/10.1121/1.4976070]

[HCS]

I. INTRODUCTION

Time reversal (TR) is a method that allows waves, generated by a single source, to be focused away from the source location at any location where a receiver can be placed.[1,2] It was first formulated in the 1960s for application in underwater acoustic communications between submarines, though it was termed "matched signal processing" at the time.[3] In the 1990s, the group of Fink *et al.* greatly expanded on the topic, for medical applications, communications, and several other applications, and they renamed it "time reversal (or reversed) acoustics." TR focusing has been used in several applications. These applications include underwater acoustics, biomedical ultrasound imaging and therapy, nondestructive evaluation, and seismology. TR was first employed in fluid media to provide underwater acoustic communication between ships,[3] and it continues to be explored and refined for this application.[4,5] In addition, as previously mentioned, time reversal has medical applications. Examples include using TR to locate and destroy a kidney stone in the body during lithotripsy treatment[6,7] and imaging teeth in dental applications.[8]

Perhaps more relevant applications of TR for the proposed demonstration are those that have been used to focus waves in elastic media. TR has been shown to be successful with a single source transducer in a silicon plate[9–11] and in glass and sandstone blocks.[12] These studies showed that a single transducer can produce energy focusing at a remote location, so long as a receiver can be placed at that location. The reverberation in a measured impulse can be exploited as a virtual array of sources during the time reversal focusing process. TR has been used to locate and characterize defects and cracks in mechanical parts,[13–26] communicate signals along pipes,[27] and in seismology to locate the epicenter of earthquakes[28] and geophysical tremor.[29]

One method of achieving time reversal focusing, sometimes termed reciprocal time reversal, obtains an impulse response between locations A and B in a sample or medium. Location A represents the location of the source. Location B represents the location of the sensor, and is where the energy focusing is desired. The impulse response is a recording of all the wave paths traversed from A to B over the time period of the recording. This impulse response is then reversed in time and broadcast from A to B (other TR methods broadcast the reversed impulse response from B to create a focus at A). The waves then retrace their original paths and are timed such that they constructively interfere at B. Reciprocal time reversal is often used in nondestructive evaluation techniques such as time reversal and nonlinear elastic wave spectroscopy (TR-NEWS) (sometimes referred to as non-linear time reversal acoustics) and the time reversed elastic nonlinearity diagnostic such as in Refs. 14–26.

The purpose of this paper is to describe procedures for developing an inexpensive demonstration of TR focusing of vibrational waves in thin plates that an educator could use to visually show the power of TR focusing in a classroom demonstration or for a laboratory exercise for her students. The authors have shown videos of this demonstration in many settings, from lectures to elementary school children, to university colloquia, to professional meetings to help convey to the audience the ability of TR to focus energy to a point away from the source transducer. The exact cost of the demonstration depends on what equipment and plates one already possesses. At the TR focal location the vibration amplitude is such that table salt (or other granular media) may be launched into the air, while the salt remains nearly in

a)Electronic mail: bea@byu.edu

contact with the plate at other spatial locations. Additionally, an object placed at the focal location can be knocked over at the time of maximal focusing. These demonstrations are achieved with a single vibration transducer that provides a concentration of energy at a remote location in the plate due to the focusing properties of TR. A scanning laser Doppler vibrometer (SLDV) is used to record the impulse response, needed for TR, at the desired focal location. Other, less-expensive, vibration sensors, such as accelerometers should be possible to use to record the impulse response. The SLDV is also used here to image the concentration of the spatial focusing at the focal location, which is not needed for the demonstrations described here. The experiments performed here are not new in terms of showing that TR can be done with a single source transducer, rather this paper attempts to describe ways to use a single channel TR experiment for demonstration purposes to visually show the result of the focusing by knocking over objects placed at the focal position or by launching salt into the air.

Time reversal focusing quality metrics are formalized here, whereas similar metrics were used previously by others.[30,31] Specifically, one metric is proposed to quantify the quality of the temporal focusing at the focal location. The peak squared amplitude is compared to the average squared amplitude over all time (before, during, and after the peak focal time). This temporal focusing quality metric is useful in situations where the focal signal is approximating a delta function. A second metric is proposed that attempts to quantify the spatial quality of the time reversal focusing by analyzing the amplitude as a function of space at the time of maximal focusing. The peak, squared amplitude is compared to the average squared amplitude over the spatial map of the focusing. Other metrics, such as reverberation time, source output efficiency, and peak frequency are explored here to show how they correlate with time reversal focusing quality.

This paper presents a technique to increase the amplitude of time reversal focusing that is different, but similar to a previously-suggested technique. Derode *et al.* proposed a one-bit time reversal technique in which only the phase information of the impulse response is used for time reversal.[32] In other words, the amplitude information of the impulse response is converted to either $+1$ or -1 values depending on whether the impulse response's instantaneous values are either positive or negative, respectively. Their experiments, conducted in a water tank, found an increase of 12 dB in the amplitude of the focus at the expense of raising the background levels (sometimes termed side lobes). The signal to noise ratio decreased as a result but the amplitude gain, combined with the compression of information makes the one-bit technique advantageous for certain applications. A variant on the one-bit technique is introduced here in which the impulse response is intentionally clipped. Intentional clipping is performed on a normalized impulse response in which a multiplication factor is applied and then information above 1 or below -1 is set equal to 1 or -1, respectively. Intentional clipping is equivalent to the one-bit procedure if the clipping multiplier is very large. One issue with the one-bit technique is that noise in the impulse response is effectively amplified relative to the signal,

though a threshold can be set to avoid one-bitting the lower amplitudes in the later part of the impulse response where the signal to noise ratio is decreased. Intentional clipping preserves some amplitude information, while taking advantage of benefits similar to the one-bit technique. Intentional clipping is a smaller contribution of this paper and a comparison of it to the one-bit technique is beyond the scope of this paper.

One educational demonstration similar to the one proposed here is the Chladni plate demonstration, in that both demonstrations provide visual identification of plate vibrations. In Chladni's demonstration, salt is sprinkled over a plate. The plate is vibrated at a resonance frequency, often using a shaker, though a violin bow may also be used.[33] The salt on the plate vibrates significantly and accumulates at the nodal lines of the modal pattern for that resonance frequency.[34,35] The TR focusing demonstration introduced here provides a short time duration focusing of energy at a single location on the plate, rather than continuous wave excitation of a mode whose amplitude is globally distributed over the plate as in Chladni's demonstration.

II. EXPERIMENTAL SETUP

In order for a single channel TR experiment to successfully provide a focus, the impulse response must contain many reflected paths between the source and the receiver. Each reflected path can be exploited to create an image source in the TR process. Thus a long reverberation time (RT60) is desirable. Six plates, of different materials which are readily available, are selected to determine which would provide the best TR focusing. Table I provides the information about the plates tested. The materials include cardboard, medium density fiberboard (MDF), particle board, steel, aluminum, and glass. The plates are somewhat similar in size, but this study's scope did not include different sizes of plates of the same material. Larger plates should provide longer reverberation times, until the point at which attenuation of the vibrations dominates, thereby yielding a decreasing reverberation time with increasing plate size. The intent here is to describe a procedure for someone to select the best plate available rather than to specify an optimal plate material and size. A larger aluminum plate, measuring $183 \times 122 \times 0.32 \text{ cm}^3$ was purchased for nearly $600 USD, and demonstrations using this plate are described in Sec. IV, however, due to its high cost it is not included in this focusing quantification study.

TABLE I. List of the plate materials used in this study, their densities, and their sizes. Mass per unit area, a commonly used quantity in structural acoustics, is obtained from the product of the density and the thickness.

Plate material	Density (kg/m³)	Length (m)	Width (m)	Thickness (mm)
Cardboard	170	0.959	1.092	6.4
MDF	760	0.787	1.201	12.7
Particle board	680	1.219	1.208	11.1
Steel	780	1537	1.092	2.0
Aluminum	2700	0.686	0.813	3.2
Glass	2500	1.016	1.524	2.4

J. Acoust. Soc. Am. **141** (2), February 2017

Heaton *et al.* 1085

The experiment is setup by placing a plate on top of six 2 cm diameter rubber stoppers to lift the plate off of a table surface, though other types of supports, made of rigid or fully elastic materials, could prove to absorb less vibrational energy. A Polytec PSV-400 scanning laser Doppler vibrometer (SLDV) is positioned above the plate and the laser spot is positioned away from the boundaries and the vibration source. A shaker, a mighty dwarf vibration speaker, is attached to a random location on the plate. Figure 1 displays a photograph of the setup. The demonstration depicted in Fig. 1 is setup on an optical table but the use of a specialized table is not necessary. The shaker is first used to broadcast a logarithmic chirp signal. This chirp signal sweeps from 500 Hz to 5000 Hz. At 500 Hz the wavelength in each plate is approximately one third of the plate's width dimension; higher frequencies create smaller TR focal regions. This chirp source waveform, $s(t)$, is generated using the following equation:

$$s(t) = \sin\left[2\pi f_0\left(\frac{k^t - 1}{\ln(k)}\right)\right], \quad (1)$$

where $f_0 = 500$ Hz and $k = 2.42$. The resulting chirp duration is 2.62 s. Above 5000 Hz the shaker's output efficiency drops off significantly. The source in each experiment that follows is the shaker, whereas the sensor in each experiment that follows is the SLDV.

The use of a chirp signal allows one to extract a higher quality impulse response than using a pulse source signal or random noise signals.[36,37] A cross correlation of the chirp signal, $s(t)$, that is broadcast from the shaker and the chirp response, $r(t)$, measured by the SLDV yields the impulse response

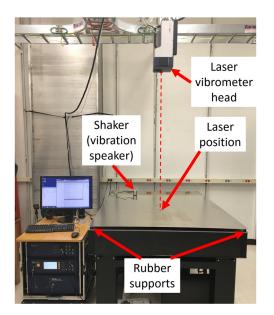$$ir(t) = \int_T s^*(\tau)r(t+\tau)d\tau, \quad (2)$$

FIG. 1. (Color online) Photograph of experiment setup with a large aluminum plate. The shaker is mounted on the upper left corner of the plate.

where T is the signal length and an asterisk represents a complex conjugate. It should be noted that measured time-domain signals are real so the complex conjugate is not needed in Eq. (2), but Eq. (2) is the general form for a cross correlation operation, which includes the case where the signals used may be complex. It should also be noted that $ir(t)$ is a *band-limited* impulse response, or Green's function between the source and the receiver, and that the amplitude of the impulse response may not have an absolute significance, but that relative differences between impulse response measurements on different plates has meaning. Figure 2 displays sample signals for the time reversal process conducted on the glass plate. Figure 2(a) shows the spectrum of $s(t)$ [the Fourier transform of $s(t)$ or $FFT\{s(t)\}$], which is a logarithmic chirp signal of duration $T = 2.62$ s starting at $t = 0.5$ s, that is sent to the source transducer. Figure 2(b) displays $r(t)$ obtained with the laser vibrometer at a selected point. Figure 2(c) show the resulting $ir(t)$ using Eq. (2). $ir(t)$ is then reversed in time [$ir(-t)$] and Fig. 2(d) displays the focal signal, $y_{TF}(t)$, obtained at the same selected point with the laser vibrometer when $ir(-t)$ is broadcast from the source. Note the difference in time scales for Figs. 2(a) and 2(b) compared to Figs. 2(c) and 2(d). Note the peak amplitude of 36.4 mm/s is 3.2 times higher than the highest peak in the chirp response signal (11.5 mm/s), showing the impulsive focusing power of the TR process.

In order to quantify a reverberation time and an output efficiency, a set of impulse responses are determined using the chirp method previously described. The SLDV sensor is placed at three different locations, while the shaker is placed at one of three different positions, distinct from the laser positions. An impulse response is determined for each sensor and source location, producing a total of nine impulse responses. For each measurement, ten time averages are used to increase the signal to noise ratio. Signal triggering is used in order to time sync the averages when the signal reaches 10% of dynamic range. A 10% pre-trigger is also used to ensure that the signal onset is recorded. For these measurements $T = 5$ s and the dynamic range is set to 10 V. The SLDV sensitivity is set to 5 mm/s/V for the chirp response recording and 125 mm/s/V for the scans of the time reversal focusing. Note that the sensitivities are taken into account when plotting signals with units of mm/s [such as in Figs. 2(b), 2(d), 3(b), 3(d), and 5].

A reverse Schroeder integration is performed on each impulse response in the set for each plate according to

$$RSI(t) = \int_t^\infty ir^2(\tau)d\tau, \quad (3)$$

where τ is the integration variable and RSI is the reverse Schroeder integration result.[38] Since real signals are finite, in practice the upper limit on the integration is the signal length, T. Since the reverberation times in some plates were very short, care was taken to avoid changes in the slope of the integration curve due to the background noise, meaning that it was not always possible to extract the decay rate from the -5 dB to -35 dB down points on the curve as specified by the room acoustics standards.[38] The $RT60$ value was
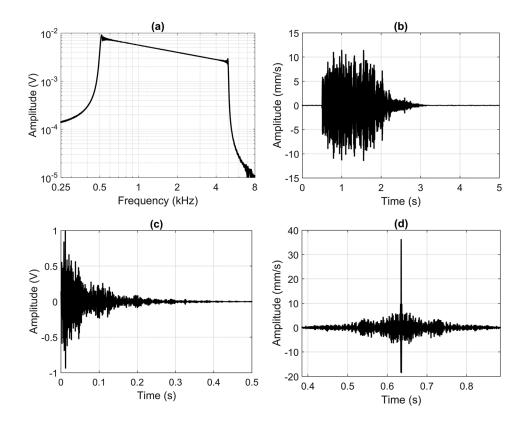
FIG. 2. Sample signals from a time reversal experiment. (a) Spectrum of the chirp signal, $FFT\{s(t)\}$, sent to the source. (b) Chirp response, $r(t)$, recorded by the laser vibrometer on the glass plate. (c) Impulse response, $ir(t)$, extracted from the cross correlation. (d) Focal signal, $y_{TF}(t)$, recorded by the laser vibrometer when the reversed impulse response is broadcast from the source.

obtained by extrapolating whatever decay amount could be reasonably determined from RSI to the amount of time it takes for the RSI to decay 60 dB from an initial value. $RT60$ is a well known quantity in architectural acoustics. For a room of volume V, surface area S, and average absorption coefficient α (bounded between 0 and 1), Eyring[39] showed that

$$RT60 = \frac{4\ln(10^6)V}{-cS\ln(1-\alpha)}, \tag{4}$$

where c is the speed of sound in air. Note that $RT60$ for a room only considers losses of energy from reflections off of walls in the room. For waves traveling in the plates considered here, similar trends for the dependence of $RT60$ on V, S, and c (though in this case it would be the speed of waves traveling in the plate medium) should follow, but α may be dependent on the inherent propagation losses in the plates rather than just dependent on losses due to boundary reflections as is the case for rooms. For plates, the ratio of V/S does not vary greatly among those tested. Thus $RT60$ should largely be inversely proportional to the speed of waves in the plates and nearly inversely proportional to α in the plates [since $-\ln(1-\alpha) \approx \alpha$ for $\alpha < 1$].

A frequency response, $H(f)$, may be calculated by taking the Fourier transform of $ir(t)$. An integration of $|H(f)|$ over the input bandwidth of 500–5000 Hz allows quantification of an output efficiency, η, representing the ratio of the vibration amplitude of the plate to the input electrical signal amplitude over the measurement bandwidth

$$\eta = \frac{1}{N}\frac{1}{S}\sum_{f=500\,\text{Hz}}^{5000\,\text{Hz}} |H(f)|, \tag{5}$$

where N is the number of frequencies summed and S is the voltage amplitude of the source signal. A peak frequency, f_P, can also be determined from a smoothed $|H(f)|$ over the input bandwidth. The wavelength of the peak frequency gives an idea of how large the focal spot's diameter may be.

The $RT60$, η, and f_P may be used to make a hypothesis about which plate material would yield the peak amplitude TR focus, A_P, and which plate would yield the highest focal quality in terms of the concentration of the focal energy in time, ξ_T, and space, ξ_S.

In order to test the relation of the abovementioned metrics to the TR performance, TR is performed on the plates. In order to quantify ξ_S, an SLDV must be used. However, since educators attempting to setup this demonstration may not have a SLDV at their disposal, it would be useful to only need to quantify the $RT60$, η, and f_P from impulse response measurements that can be measured at a single point with a laser vibrometer or a cheaper vibration sensor, such as an accelerometer. Thus a scan of the time reversal focusing on each of the plates is conducted to see how the impulse response metrics correlate with the time reversal performance metrics A_P, ξ_T, and ξ_S. These metrics are similar to those proposed by one of the authors and others previously.[30,31]

For a spatial scan of a TR focusing wave field, the data set would consist of N_X by N_Y time signals, $A(x, y, t)$. The A_P is the maximum of the absolute value of the temporal focal signal, $A(x_0, y_0, t)$, which is measured at the focal position (x_0, y_0). The temporal focal quality of a TR experiment is

$$\xi_T = \frac{[A_P]^2}{\frac{1}{N}\int_0^T [A(x_0, y_0, t)]^2 dt}, \tag{6}$$
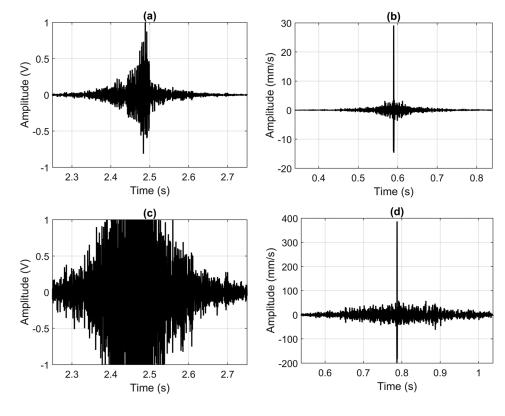
where the integration of each discrete time step between 0 and T is included. Thus a delta function signal, representing an ideal-though-impossible TR signal, would have a value $\xi_T = N$. A sine wave signal, where the peak amplitude is no larger than other peaks in the signal, would have a value $\xi_T = 2$ for large N. As a final example, a flat line of any magnitude would have a value of $\xi_T = 1$, because the peak is equal to the average value. At the focal time (the time of maximal vibration), T_f, the data set is reduced to a map in space at T_f, or $A(x, y, T_f)$. The spatial focal quality of a TR experiment is

$$\xi_S = \frac{[A_P]^2}{\dfrac{1}{N_X N_Y} \displaystyle\int_1^{N_Y} \int_1^{N_X} [A(x, y, T_f)]^2 dx dy}. \tag{7}$$

The deconvolution technique, or inverse filter, applied to TR has been shown to produce a sharper TR focus, often at the expense of TR focal amplitude.[40–43] In the context of the goal of this demonstration, a large A_P is desired but high values of ξ_T and ξ_S are desired also. Additionally, the TR signal that will be broadcast may be intentionally clipped in order to increase the focal amplitude. In some cases, the direct arrival or early reflections in an impulse response are at much higher amplitudes than the later arrivals in the impulse response. The result is that the TR focusing of such a reversed impulse response is dominated by only the direct arrival and early reflections. When the reversed impulse response (TR signal) is clipped the timing of the impulse response's many arrivals are preserved, but the direct arrival and early reflections no longer dominate the TR signal, but now the later reflections are higher in amplitude (higher

amplitude in a relative sense) to the direct arrival and early reflections, such that the later reflections can now contribute more to yield a higher amplitude focus. To intentionally clip the TR signal, one can start by normalizing the TR signal and then multiplying it by a desired number, C. Then every positive TR signal value that exceeds C is set equal to C, while every negative TR signal value that is less that $-C$ is set equal to $-C$. For the glass plate various values of C (ranging from $C = 2$ to $C = 100$) were used to determine an optimal $C = 10$ in terms of maximizing A_P while minimizing the corruption of ξ_T as happens with increasing C. At higher values of C, A_P no longer increases and instead ξ_T decreases significantly. The optimal value of C likely depends on a given experiment's parameters (such as $RT60$).

Figure 3 illustrates the effects of incorporation deconvolution and clipping to the focal signal, $y_{TF}(t)$. For the deconvolution signal $A_P = 29.1$ mm/s compared to $A_P = 36.4$ mm/s for standard TR (without deconvolution), representing a reduction of 20% in peak amplitude. The shaker has internal amplification, which increases the peak amplitude by a factor of 3.6 relative to its default excitation level. When the deconvolution signal is clipped ($C = 10$) and amplified, the $A_P = 386.8$ mm/s, representing a gain of a factor of 13.3 over the deconvolution $y_{TF}(t)$ without clipping and amplification. It also represents a gain of 10.6 over the standard $y_{TF}(t)$ without clipping and amplification. When standard TR is clipped and amplified, the resulting ξ_T is noticeably lower than when deconvolution TR is clipped and amplified, though the A_P is slightly higher with standard TR. Clearly more energy (total amplitude over time) is broadcast in the signal displayed in Fig. 3(c) than in Fig. 3(a). The TR focal quality, ξ_T, is also noticeably decreased in Fig. 3(d) relative

FIG. 3. Deconvolution time reversal (TR) signals obtained on the glass plate. (a) Deconvolution TR signal without clipping. (b) Deconvolution TR focal signal without clipping. (c) Deconvolution TR signal with 10 times clipping. (d) Deconvolution TR focal signal with 10 times clipping.

to Fig. 3(b), though the peaks of energy away from the main focus are approximately the same amplitude in relation to the main focal peak for the signals in both figures.

The TR focusing occurs at the location where the chirp response is recorded. Scans of the velocity wave fields during TR focusing are done with the SLDV. The same settings of the laser vibrometer with regards to sensitivity, triggering, and maximum response were used in this part of the experiment as used previously. For the scans of TR focusing in each plate, the deconvolution technique, signal clipping (times 10), and amplification are used.

III. RESULTS

The scans of the TR focusing wave fields on each plate are done with a 27 by 37 point scan grid, where the spacing between each scan point is 2.0 cm. As previously stated, a deconvolution is applied to the impulse response signal. The deconvolution signal is then intentionally clipped by a factor of 10 and sent by the shaker into the plate. Three time averages are used for each scan point. Developer spray was applied to each plate surface to enhance the reflectivity of the laser light. Figure 4 displays the spatial distribution of the TR focusing at the time of peak focusing (the value at each point in space is squared to represent a map of the instantaneous energy). Somewhat surprisingly, the TR
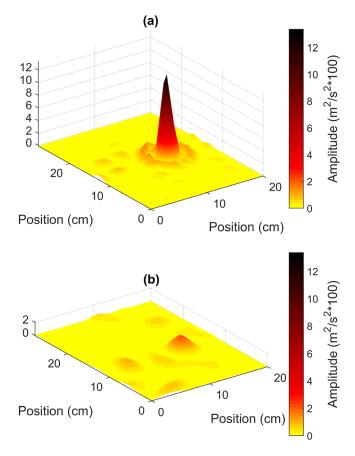

FIG. 4. (Color online) Spatial maps of the instantaneous energy at the time of peak time reversal focusing. (a) Glass plate. (b) Cardboard plate. Color denotes amplitude. The peak heights are to scale with respect to each other (meaning 2 units on the z-axis is the same for both plots).

focusing achieved in each plate material was fair, including in the cardboard and wooden plates, in terms of the presence of a spatially localized momentary increase of energy at the intended focal location. The authors did not initially expect to get a TR focus in highly damped material such as cardboard. Figure 4 illustrates the vast improvement of the spatial confinement of the focusing in the glass plate as compared to that in the cardboard plate and also the much higher A_P in the glass than in the cardboard.

The impulse response metrics of $RT60$, η, and f_P are given in Table II. These values represent average values computed from each of the nine impulse response signals in the set for each plate. The TR focal signal quality metrics of A_P, ξ_T, and ξ_S are also given in Table II. The best TR focusing occurs in the glass plate and the worst TR focusing occurs in the cardboard plate. Even though the cardboard plate yielded a slightly higher η value than the glass plate did, the time reversal focal amplitude, A_P, is 2.6 times higher in the glass plate than in the cardboard plate. Thus, the output efficiency η value is not a good indicator of the amplitude of the TR focusing by itself. The plates listed in Table II are approximately listed in order of increasing $RT60$. When comparing the ξ_T and ξ_S metrics, the glass plate outperformed the cardboard plate by a factor of 2.8 and 5.1, respectively, and the glass plate's metrics were highest among all plates. It appears that the TR focusing quality, whether in space or time, is correlated with the $RT60$. The correlation of TR focusing quality and $RT60$ is to be expected since more reflections used in the TR process provide more virtual sources that contribute to the TR focusing. The combination of high η and $RT60$ values yields both a large amplitude focus and a spatially constrained focus. The steel and aluminum plates also had high $RT60$ values, in fact values higher than in glass, but they yielded lower TR focusing quality values. The aluminum plate's performance was nearly as good as that of the glass plate, but its cost is on the order of 6 times higher than a glass plate of comparable size. Despite the higher cost of the aluminum plate, it is not as fragile as a glass plate and this should be taken into consideration.

IV. DEMONSTRATION

The evolution of TR focusing from the SLDV can be visualized using Polytec's PSV software. Figure 5 shows five frames that display the evolution of the focusing in space along with the temporal signal recorded at the focal location. The dashed lines indicate the instants in time for the spatial images on the left. The positive phase circular wave fronts visible in the upper two spatial images are traveling inward

TABLE II. Table of $RT60$, η, f_P, A_P, ξ_T, and ξ_S.

	$RT60$ (s)	η (arb. units)	f_P (Hz)	A_P (m/s)	ξ_T	ξ_S
Cardboard	0.13	29.0	510	0.135	213	13.3
MDF	0.16	3.79	770	0.037	246	18.3
Particle board	0.18	4.73	880	0.043	329	23.8
Steel	0.79	1.00	1022	0.158	322	60.5
Aluminum	0.85	16.7	990	0.273	204	30.9
Glass	0.78	27.7	1090	0.365	602	68.2

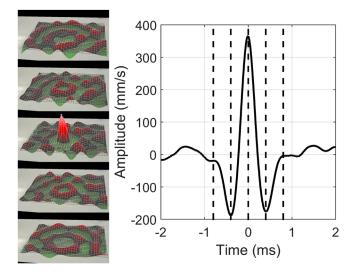J. Acoust. Soc. Am. **141** (2), February 2017

Heaton *et al.* 1089

FIG. 5. (Color online) Evolution of the time reversal focusing over time. Spatial maps at different time intervals (left) and focal signal at focal location (right). Dashed lines indicate times corresponding to the spatial maps.
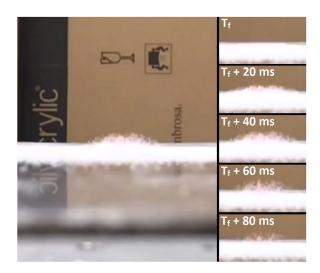

FIG. 6. (Color online) Photograph of salt jump visualization at the time of peak salt displacement (left) and snapshots at the time of focus and afterwards (right).

toward the focal location. The positive phase circular wave fronts visible in the lower two spatial images are traveling outward away from the focal location. Polytec's software provides a movie of the wave propagation that clearly shows the converging waves that constructively interfere at the focal location and then diverge away. This section describes some ways to visualize the impulsive focusing power of TR.

A visualization of the focusing may be done by sprinkling salt on the plate after the chirp response signal has been recorded. When the waves coalesce at the focus location and constructively interfere, the plate vibrates significantly at that location. Figure 6 shows a photograph, taken with a high speed camera (iPhone 6S at 200 frames/s, or 0.005 ms between frames), when the salt is thrown up into the air at its maximum height. An object is thrown off of the plate when the plate is moving upward and the downward acceleration exceeds that of the acceleration due to gravity, $g = 9.8 \, \text{m/s}^2$. The peak velocity of the plate occurs when the plate's acceleration is zero and decreasing. If the velocity signal changes quickly enough, then the plate's acceleration is less than $-g$ (more negative), very soon after the peak velocity. The peak velocity occurs at the focal time T_f and thus the object can be thrown off of the plate essentially at T_f, assuming the velocity is changing rapidly enough. Also shown in Fig. 6 are progressive photographs of the salt over time from T_f to $T_f + 80 \, \text{ms}$. The salt is thrust upward 2 cm above the plate. Assuming the salt is undergoing projectile motion, the initial velocity, v_0, of the salt should equal $v_0 = \frac{1}{2} g t$, where t is the time in which the salt is thrown upward until it returns to the plate. Frame by frame video analysis shows that $t = 80 \, \text{ms}$, then $v_0 = 400 \, \text{mm/s}$, which is close to the peak velocity measured by the laser vibrometer of $A_P = 365 \, \text{mm/s}$. If a time derivative of the velocity signal in Fig. 5 is applied, then the peak negative acceleration is $-2400 \, \text{m/s}^2$ (247 times the acceleration due to gravity), which occurs at approximately 0.5 ms in Fig. 5. This confirms that the acceleration is lower than $-g$ very soon after T_f. A multimedia video, Mm. 1, shows the salt being thrown off of

the plate in real time and then in slow motion. The video allows visualization of the spatial extent of the focusing.

Mm. 1. Video of the salt being thrown off of the plate during time reversal focusing. The video is first played in real time followed by a slow motion playback. This is a file of type "mov" (2.7 Mb).

Another demonstration that works fairly well, though not always repeatable, is to setup an object that is stiff and lightweight at the focal position so that it may be thrust into the air and knocked over. Figure 7 displays images of a few different items being knocked over when they are placed at the focal position for the glass plate and also on an aluminum plate larger than that studied previously in this paper. The larger aluminum plate measures $183 \times 122 \times 0.32 \, \text{cm}^3$ and is not included in the preliminary study since its cost was nearly $600.00 USD, which is deemed too expensive to recommend for this demonstration, whereas the aluminum plate studied earlier is a scrap piece of aluminum. We have found that small wooden corks (mass = 0.34 g), small cardboard cylinders (mass = 3.4 g), and lighter weight cable adapters (mass = 4.0 g) can be knocked over at the focal position repeatedly while not being knocked over anywhere else on the plate at least 10 cm from the focal position. Lego minifigures (mass = 3.1 g) are appealing for this demonstration to get the attention of children, but the minifigures are somewhat unstable and while the Lego minifigure setup at the focal position is the most likely to be knocked over, sometimes it does not get knocked over. Additionally, the Lego minifigures setup at locations away from the focal position sometimes get knocked over, though less frequently. In each of the photos depicted in Fig. 7, the inset image shows the undisturbed state of the object prior to the focusing while the background image is of the object being thrown into the air before being knocked over. In the case of the Lego minifigures, all of the figures move during the focusing but only the figure in the middle of the photo is knocked off of his feet. In the case of Figs. 7(a) and 7(b), the
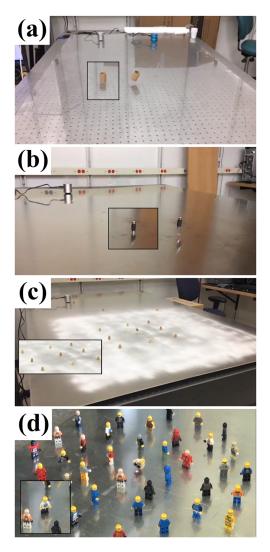
FIG. 7. (Color online) Photographs of time reversal focusing being used to knock over objects. The inset image, outlined in black, shows the undisturbed state. (a) A cardboard cylinder is knocked over on the glass plate. (b) An RCA adapter, (c) wooden cork (developer spray was applied to allow laser scanning), and (d) Lego minifugure are knocked over on the large aluminum plate.

focusing can be repeated successively as the object (cardboard cylinder and cable adapter) is placed at different locations on the plate. Even if the object is placed near the source the vibrations are not large enough to knock over the object unless it is placed at the focal location. A video of several demonstrations of objects being knocked over may be viewed in Mm. 2. The first portion of the video shows the response of a cardboard tube as it is placed at multiple locations, even next to the source, while the reversed impulse response is broadcast for each cardboard tube placement. The tube is only knocked over when it is placed at the focal signal (where the impulse response was obtained). After this portion of the video, several other demonstrations of objects being knocked over in slow motion are shown.

Mm. 2. Video of several demonstrations of objects being knocked over by time reversal focusing, some in real time and some in slow motion. This is a file of type "mov" (36.7 Mb).

An important consideration that remains to be addressed in order to keep this demonstration from being overly expensive is the vibration sensor. The demonstrations shown here have employed a laser Doppler vibrometer (LDV), which cost tens of thousands of U.S. dollars at minimum (lasers with scanning capabilities are in the hundreds of thousands of dollars range). The LDV directly senses velocity as a function of time. Thus, if a position or acceleration versus time sensor is used, then the higher frequencies will be under represented or over represented, respectively, relative to lower frequencies in comparison to velocity sensors. We recommend the use of inexpensive accelerometers as a cheap vibration sensing option. The dominant frequencies used in these demonstrations were in the neighborhood of 1000 Hz, so frequency bandwidth and the sensitivity of the sensor should be considered.

V. CONCLUSION

This paper has described a demonstration of spatially-confined, time reversal focusing of vibrations in thin plates using a single source transducer and a single receiver. The focusing performance metrics (peak amplitude, spatial quality, and temporal quality) indicate that the $1016 \times 1524 \times 2.4 \, mm^3$ glass plate was the best plate for a demonstration. Metrics that quantify properties of the impulse response in a plate were described. It was found that the combination of high reverberation time and sensitivity metrics are a good indicator of spatially localized focusing and large amplitude focusing. Some plates had high reverberation times but low efficiencies (aluminum and steel plates), while the cardboard plate had a high efficiency but a low reverberation time, and in each of these cases the focusing performance was weaker than in the glass plate. The glass plate had a reverberation time of 0.78 s and its efficiency was comparable to cardboard and nearly twice the efficiency of the aluminum plate. In addition, glass is significantly less expensive and more accessible than aluminum, which gave the next best focusing performance. It is worth noting that glass plates must be handled with great care to avoid inadvertent shattering of the glass, whereas an aluminum plate would not shatter if it was dropped.

A deconvolution operation was employed to provide a sharp focusing in time. Focusing amplitude was found to be enhanced by a factor of up to 13.3 when the time reversed deconvolution signal was intentionally clipped by a factor of 10 prior to amplifying and broadcasting the signal to create the focusing. A peak velocity of 365 mm/s was achieved in the glass plate along with a peak acceleration of 247 times the acceleration due to gravity.

Salt was sprinkled onto the glass plate and the focusing demonstration was used to make the salt visibly jump off of the plate only at the selected focusing location. Additionally, demonstrations of the ability of time reversal to knock over objects was shown, including knocking over cardboard cylinders, cable adapters, wooden corks, and Lego minifigures. The salt jumping demonstration may be the best live demonstration since the observer can clearly see the localized nature of the high amplitude focusing of elastic waves in a

J. Acoust. Soc. Am. **141** (2), February 2017

Heaton *et al.* 1091

plate. The Lego minifigures were not knocked over consistently enough to provide a reliable demonstration due to their inherent instabilities.

Further research should explore the effect of the plate thickness and plate size of the focusing performance since it is expected that the reverberation time, for larger plates in particular, will vary with the dimensions of the plate. Additionally, this research did not focus on the use of an inexpensive vibration sensor and further work could compare the use an accelerometer to a laser Doppler vibrometer. Finally, one might easily employ two source transducers from their computer's stereo outputs to produce a larger and more spatially confined focus of energy.

ACKNOWLEDGMENTS

[1]M. Fink, "Time reversed acoustics," Phys. Today **50**(3), 34–40 (1997).

[2]B. E. Anderson, M. Griffa, C. Larmat, T. J. Ulrich, and P. A. Johnson, "Time reversal," Acoust. Today **4**(1), 5–16 (2008).

[3]A. Parvulescu and C. Clay, "Reproducibility of signal transmission in the ocean," Radio Electron Eng. **29**(4), 223–228 (1965).

[4]C. He, Q. Zhang, and J. Huang, "Passive time reversal communication with cyclic shift keying over underwater acoustic channels," Appl. Acoust. **96**(9), 132–138 (2015).

[5]G. Zhang, J. M. Hovem, D. Hefeng, and L. Liu, "Coherent underwater communication using passive time reversal over multipath channels," Appl. Acoust. **72**(7), 412–419 (2011).

[6]M. Fink, "Time-reversal acoustics in biomedical engineering," Ann. Rev. Biomed. Eng. **5**(1), 465–497 (2003).

[7]M. Fink, "Time reversal and phase conjugation with acoustic waves: Industrial and medical applications," Lasers Electro-Opt. **3**, 2334–2335 (2005).

[8]S. Dos Santos and Z. Prevorovsky, "Imaging of human tooth using ultrasound based chirp-coded nonlinear time reversal acoustics," Ultrason. **51**(6), 667–674 (2011).

[9]C. Draeger and M. Fink, "One-channel time reversal of elastic waves in a chaotic 2D-silicon cavity," Phys. Rev. Lett. **79**, 407–410 (1997).

[10]C. Draeger and M. Fink, "One-channel time-reversal in chaotic cavities: Theoretical limits," J. Acoust. Soc. Am. **105**(2), 611–617 (1999).

[11]C. Draeger, J.-C. Aime, and M. Fink, "One-channel time-reversal in chaotic cavities: Experimental results," J. Acoust. Soc. Am. **105**(2), 618–625 (1999).

[12]A. M. Sutin, J. A. Ten Cate, and P. A. Johnson, "Single-channel time reversal in elastic solids," J. Acoust. Soc. Am. **116**(5), 2779–2784 (2004).

[13]C. Prada, E. Kerbrat, D. Cassereau, and M. Fink, "Time reversal techniques in ultrasonic nondestructive testing of scattering media," Inv. Problems **18**(6), 1761–1773 (2002).

[14]T. Goursolle, S. Callé, S. Dos Santos, and O. BouMatar, "A two-dimensional pseudospectral model for time reversal and nonlinear elastic wave spectroscopy," J. Acoust. Soc. Am. **122**(6), 3220–3229 (2007).

[15]B. E. Anderson, M. Griffa, T. J. Ulrich, P.-Y. Le Bas, R. A. Guyer, and P. A. Johnson, "Crack localization and characterization in solid media using time reversal techniques," in *44th US Rock Mechanics Symposium and 5th U.S.–Canada Rock Mechanics Symposium*, Salt Lake City, UT (June 2010).

[16]B. Van Damme, K. Van Den Abeele, Y. Li, and O. BouMatar, "Time reversed acoustics techniques for elastic imaging in reverberant and nonre-verberant media: An experimental study of the chaotic cavity transducer concept," J. Appl. Phys. **109**(10), 104910 (2011).

[17]B. Van Damme, K. Van Den Abeele, and O. BouMatar, "The vibration dipole: A time reversed acoustics scheme for the experimental localisation of surface breaking cracks," Appl. Phys. Lett. **100**(8), 084103 (2012).

[18]H.-J. Jeong and D. Barnard, "Nonlinear time reversal focusing and detection of fatigue crack," J. Korean Soc. Nondest. Test. **44**(8), 355–361 (2012).

[19]F. Ciampa and M. Meo, "Nonlinear elastic imaging using reciprocal time reversal and third order symmetry analysis," J. Acoust. Soc. Am. **131**(6), 4316–4323 (2012).

[20]A. S. Gliozzi, M. Scalerandi, and P. Antonaci, "One-channel time reversal acoustics in highly attenuating media," J. Phys. D: Appl. Phys. **46**(13), 135502 (2013).

[21]J. Zhu, Y. Zhang, and X. Liu, "Simulation of multi-cracks in solids using nonlinear elastic wave spectroscopy with a time-reversal process," Wave Motion **51**(1), 146–156 (2014).

[22]P. Y. Le Bas, M. C. Remillieux, L. Pieczonka, J. A. Ten Cate, B. E. Anderson, and T. J. Ulrich, "Damage imaging in a laminated composite plate using an air-coupled time reversal mirror," Appl. Phys. Lett. **107**(18), 184102 (2015).

[23]S. Delrue, K. Van Den Abeele, and O. BouMatar, "Simulation study of a chaotic cavity transducer based virtual phased array used for focusing in the bulk of a solid material," Ultrason. **67**, 151–159 (2016).

[24]E. L. Villaverde, S. Robert, and C. Prada, "Ultrasonic imaging of defects in coarse-grained steels with the decomposition of the time reversal operator," J. Acoust. Soc. Am. **140**(1), 541–550 (2016).

[25]M. Lints, S. Dos Santos, and A. Salupere, "Solitary waves for non-destructive testing applications: Delayed nonlinear time reversal signal processing optimization," Wave Motion in press (2016).

[26]P. Blanloeuil, L. R. F. Rose, J. A. Guinto, M. Veidt, and C. H. Wang, "Closed crack imaging using time reversal method based on fundamental and second harmonic scattering," Wave Mot. **66**, 156–176 (2016).

[27]B. E. Anderson, T. J. Ulrich, P.-Y. Le Bas, and J. A. Ten Cate, "Three dimensional time reversal communications in elastic media," J. Acoust. Soc. Am. **139**(2), EL25–EL30 (2016).

[28]C. S. Larmat, R. A. Guyer, and P. A. Johnson, "Time-reversal methods in geophysics," Phys. Today **63**(8), 31–35 (2010).

[29]C. S. Larmat, R. A. Guyer, and P. A. Johnson, "Tremor source location using time-reversal: Selecting appropriate imaging field," Geophys. Res. Lett. **36**(22), L22304, doi:10.1029/2009GL040099 (2009).

[30]T. J. Ulrich, B. E. Anderson, P.-Y. Le Bas, C. Payan, J. Douma, and R. Snieder, "Improving time reversal focusing through deconvolution: 20 questions," Proc. Meet. Acoust. **16**, 045015 (2012).

[31]B. E. Anderson, T. J. Ulrich, and P.-Y. Le Bas, "Imaging crack orientation using the time reversed elastic nonlinearity diagnostic with three component time reversal," Proc. Meet. Acoust. **19**, 065069 (2013).

[32]A. Derode, A. Tourin, and M. Fink, "Ultrasonic pulse compression with one-bit time reversal through multiple scattering," J. Appl. Phys. **85**(9), 6343–6352 (1999).

[33]T. Neilsen, W. J. Strong, K. L. Gee, B. E. Anderson, S. D. Sommerfeldt, and T. W. Leishman, "Creating an active-learning environment in an introductory acoustics course," J. Acoust. Soc. Am. **131**(3), 2500–2509 (2012).

[34]H. J. van Gerner, K. van der Weele, M. A. van der Hoef, and D. van der Meer, "Air-induced inverse Chladni patterns," J. Fluid Mech. **689**, 203–220 (2011).

[35]T. D. Rossing, "Chladni's law for vibrating plates," Am. J. Phys. **50**, 271–274 (2010).

[36]P. S. Kovitz and F. M. Becker, "Time delay spectrometry and maximum-length sequence measurements: A comparison in practical applications," in *95th Convention of the Audio Engineering Society*, Preprint 3702, New York (1993).

[37]S. Muller and P. Massarani, "Transfer-function measurement with sweeps," J. Audio Eng. Soc. **49**(6), 443–471 (2001), available at http://www.aes.org/e-lib/browse.cfm?elib=18530.

[38]ISO 3382:1997(E), *Acoustics—Measurement of the Reverberation Time of Rooms with Reference to other Acoustical Parameters* (International Organization for Standardization, Geneva, Switzerland, 1997).

[39]C. F. Eyring, "Reverberation time in 'dead' rooms," J. Acoust. Soc. Am. **1**, 217–241 (1930).

[40]M. Tanter, J.-L. Thomas, and M. Fink, "Time reversal and the inverse filter," J. Acoust. Soc. Am. **108**, 223–234 (2000).

[41]M. Tanter, J. F. Aubry, J. Gerber, J.-L. Thomas, and M. Fink, "Optimal focusing by spatiotemporal filter. I. Basic principles," J. Acoust. Soc. Am. **110**, 37–47 (2001).

[42]T. Gallot, S. Catheline, P. Roux, and M. Campillo, "A passive inverse filter for Green's function retrieval," J. Acoust. Soc. Am. **131**, EL21–EL27 (2011).

[43]B. E. Anderson, J. Douma, T. J. Ulrich, and R. Snieder, "Improving spatio-temporal focusing and source reconstruction through deconvolution," Wave Motion **52**, 151–159 (2015).